New York, 1963).
[6]W. H. Potter, Rev. Sci. Instr. 42, 618 (1971).
[7]W. H. Potter, thesis (University of Illinois, 1970) (unpublished).
[8]C. Ryter, Nucl. Instr. Methods 49, 267 (1967).
[9]W. H. Potter, Phys. Rev. B (to be published).
[10]J. P. Wolfe and C. D. Jeffries, Phys. Rev. B 4, 731 (1971).
[11]K. H. Langley, thesis (University of California, Berkeley, 1966) (unpublished).
[12]P. V. E. McClintock and H. M. Rosenberg, Pure Appl. Cryogenics 4, 107 (1965); *Proceedings of the International Institute of Refrigeration, Commission 1 Grenoble*, 1965 (Pergamon, New York, 1965).
[13]H. Glättli, Can. J. Phys. 46, 103 (1968).
[14]H. K. Frederking, J. Am. Inst. Chem. Engrs. 64, 21 (1968).
[15]H. Meyer and P. L. Smith, J. Phys. Chem. Solids 9, 285 (1958).
[16]V. A. Atsarkin, Zh. Eksperim. i Teor. Fiz. 53, 222 (1967) [Sov. Phys. JETP 26, 149 (1968)].
[17]See, e.g., B. W. Faughnan and W. P. Strandberg, J. Phys. Chem. Solids 19, 155 (1961); or P. L. Scott and C. D. Jeffries, Phys. Rev. 127, 32 (1962).
[18]LJ did, in fact, see a small proton polarization enhancement using a single crystal of LMN:Ce in a rotating-sample spin refrigerator. However, in a polycrystalline sample, very few of the crystallites will be oriented such that the crystal $c$ axis ever becomes parallel to $H$.

PHYSICAL REVIEW B VOLUME 5, NUMBER 5 1 MARCH 1972

# Determination of the Thermal Diffuse Scattering at the Bragg Reflections of Si and Al by Means of the Mössbauer Effect

G. Albanese and C. Ghezzi
*Istituto di Fisica dell'Università, Parma, Italy*
and
A. Merlini and S. Pace
*Solid State Physics, Physics Division, C. C. R. Euratom, Ispra, Italy*
(Received 7 September 1971)

The 14.4-keV $\gamma$ rays from $Co^{57}$ sources were scattered on different crystallographic planes of various Si and Al crystals. By using nuclear resonance absorption it was possible to separate the elastic and inelastic components of the scattered beams. An analysis of the nuclear resonance absorption peak on the beam diffracted by the {555} planes of Si and a double Bragg-scattering experiment support the expectation that the elastic component of the scattered beam is due to Bragg diffraction. The angle dependence of the relative intensities of the inelastic parts at various Bragg peaks of Si and Al crystals, corrected for the contributions of Compton scattering, were in satisfactory agreement with the angle dependence calculated on the basis of the lattice wave theory of thermal diffuse scattering. These calculations were simplified by assuming that the crystals were elastically isotropic and that the reciprocal lattice volume, over which the thermal scattering was integrated, had either a spherical or cylindrical shape. Good agreement between theory and experiment was found for the temperature dependence of the thermal scattering intensity at the {444} and {555} diffraction peaks of silicon, between 80 and 600°K.

## I. INTRODUCTION

The x-ray measurements of the integrated intensities of Bragg reflections can be easily corrected for the contributions of fluorescence and Compton scatterings, because the intensities of these scatterings vary slowly in reciprocal space and can be simply subtracted. The first-order thermal diffuse scattering (TDS) instead peaks strongly at the reciprocal lattice nodes, for vanishing energy and momentum of the acoustic phonons, and can be only partially eliminated by the usual background correction. This poses a problem when accurate values of the diffracted intensities are required; in fact, the relative amount of the TDS depends on the geometry of the scattering experiment and increases with the order of reflection. An evaluation of the TDS correction is quite difficult in practice, as shown in a review paper by Cochran.[1] A number of methods have been recently developed by making simplifying assumptions about some of the various parameters which can affect the intensity contribution of thermal scattering to the Bragg peak.[2-4] However, a comparison of the results of the calculations with experimental data is missing. The change in energy of the TDS radiation is only a few parts per million and there is no hope to eliminate this inelastic contribution from the elastic diffraction peaks by using the conventional techniques of x-ray diffraction.

The possibility of using a method of thermal neutron elastic diffraction to separate the background of thermal scattering from the Bragg peaks was examined. This method used a triple-axis spectrometer of the type employed in the determination of phonon-dispersion curves. Unfortunately, the energy resolution of the spectrometer was of the order of 1 meV, so that only the contributions of the scattering by phonons of an energy greater than 1 meV were eliminated. The intensity peak under the Bragg line, due to scattering by low-energy acoustic phonons, was not removed from the Bragg intensity.[5]

A solution of the above problem is given by the application of the Mössbauer effect. The recoilless emission and absorption of low-energy $\gamma$ rays, combined with the high selectivity of the phenomenon of nuclear resonance absorption, permits an energy resolution as small as a few $10^{-8}$ eV. Other authors have applied such a method to the separation of the thermal diffuse scattering at the {200} and {400} Bragg peaks of a LiF crystal.[6] We have previously described the application of the same technique to study the {444} and {555} reflections of silicon.[7] In the present work the technique has been applied to the investigation of the angle and temperature dependence of the TDS intensity for various reflections of Si and Al.

## II. EXPERIMENTAL METHOD

The experimental technique which was described in a previous paper[7] is briefly summarized below. Only the most important modifications and some considerations on the precision of the scattered-intensity measurements are discussed with some detail. Experiments were done in both the Bragg (reflection) and Laue (transmission) geometries.

Figure 1 illustrates the geometry of the scattering experiment in the Bragg case. Two $Co^{57}$ Mössbauer sources, of 100-mCi nominal activity, were used for the present work. One source was $Co^{57}$ diffused in a 50-$\mu$m-thick copper foil; the other was $Co^{57}$ diffused in a chromium platelet. The active area of the sources was rectangular in shape, 0.5 cm wide by 1 cm high. The absorber was a foil of 310 stainless steel, 98% enriched in $Fe^{57}$, with a thickness equal to 1 mg/cm$^2$ of $Fe^{57}$. The advantage of the source with the chromium matrix is that source and absorber are very close to the peak of the nuclear resonance when both of them are at rest. The use of mechanical or electromechanical transducers can thus be avoided, the experimental technique is considerably simplified, and there is an appreciable reduction in the counting times with the absorber at resonance. This time gain is particularly attractive because the intensities of the scattered beams are very weak. In the case of the source with the copper matrix the absorber is at resonance with the source when driven with a velocity of +0.035 mm/sec (the positive sign refers to motion of the absorber away from the source). The detector was a NaI thallium-activated scintillation crystal in the form of a disk, about 2.5 cm in diameter and 0.02–0.03 cm thick. Although a single-channel pulse-height analyzer was used to discriminate the photons of 14.4 keV, a thin scintillation crystal was necessary in order to reduce the background (mostly due to the $\gamma$ rays of energy equal to 122 keV). The detector was shielded with lead against cosmic radiation. The ambient and electronic background was less than 3 counts/min.

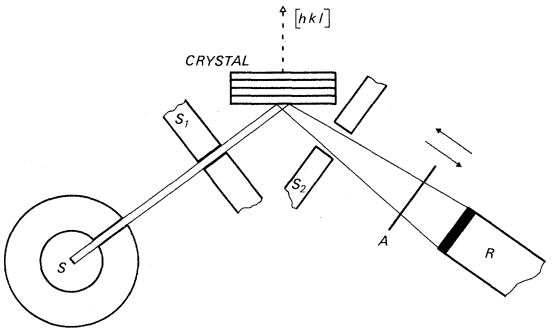


FIG. 1. Scheme of the geometry of the scattering experiments in the symmetrical Bragg case. $S$ and $A$ are the Mössbauer source and absorber, respectively. $S_1$, the rectangular slit on the incident beam, has dimensions about equal to those of the active area of the source. $R$ is the scintillation detector.

The separation of the $\gamma$ rays which are elastically scattered by the crystal from those which suffer inelastic scattering is done by using the following procedure. Let $I_\infty(2\theta)$ and $I_R(2\theta)$ be the intensities of the $\gamma$ rays scattered at the angle $2\theta$ with source and absorber out of and in resonance, respectively. The following ratio is proportional to the fraction of recoilless $\gamma$ rays which are scattered elastically by the crystal:

$$P_{2\theta} = \frac{I_\infty(2\theta) - I_R(2\theta)}{I_\infty(2\theta)} .$$

The corresponding ratio $P_0$ on the direct beam from the source (with the crystal removed from the beam) is proportional to the fraction of $\gamma$ rays which undergo recoilless emission and resonant absorption, and is a characteristic of the source-absorber combination. The expressions $P_{2\theta}/P_0$ and $1 - P_{2\theta}/P_0$ are, then, the fractions of the incident radiation which are scattered elastically and inelastically, respectively, by the crystal. The validity of these statements was verified experimentally, as explained in Sec. III. The intensities $I_{el}$ and $I_{in}$ of the elastic and inelastic scatterings are given by the

following formulas:

$$I_{el} = \frac{P_{2\theta}}{P_0} I_\infty(2\theta) = \frac{I_\infty(2\theta) - I_R(2\theta)}{P_0} ,$$
$$I_{in} = \left(1 - \frac{P_{2\theta}}{P_0}\right) I_\infty(2\theta) = I_\infty(2\theta) - I_{el} . \quad (1)$$

In this type of work the replacement of the x-ray tube with a Mössbauer source poses difficulties with respect to the counting rate. At the Bragg peak for high-order reflections and in regions away from the nodes of the reciprocal lattice, the scattered intensities are very low. For instance, at the boundary of the Brillouin zone, along the line connecting the (220) and (440) nodes of the reciprocal lattice, the intensity of the 14.4-keV radiation is of the order of 3–5 counts/min (according to the age of the source). Therefore, one should try to optimize all the factors relevant to the measurements of the scattered intensity, such as the total and specific activities of the source, the combination of the source and the absorber, and the choice of the detector. Some of these problems and their potential solutions are discussed by other authors.[8] We will examine here the precision which can be obtained in the determination of $I_{el}$ and $I_{in}$. The errors $\Delta I_{el}$ and $\Delta I_{in}$ due to the statistical error in the number of counts, which are accumulated to obtain $I_\infty$ and $I_R$, are given by

$$\Delta I_{el} = \left(\frac{I_\infty(2\theta)}{t_\infty P_0^2} + \frac{I_R(2\theta)}{t_R P_0^2}\right)^{1/2} ,$$
$$\Delta I_{in} = \left(\frac{I_\infty(2\theta)}{t_\infty} + (\Delta I_{el})^2\right)^{1/2} , \quad (2)$$

where $t_\infty$ and $t_R$ are the counting times with the absorber out of and in resonance. The statistical error in a number of counts $N$ was taken equal to $\pm\sqrt{N}$. It was verified that different measurements of the same quantity did satisfy the statistical accuracy rule for the number of counts. It was also assumed that $P_0$ is known with great precision, since there is no time difficulty in collecting high numbers of counts on the direct beam. Let us first consider the contribution to the error $\Delta I_{el}$ by the number of counts with the absorber out of resonance. It is clear from the above formula that the time $t_\infty$ necessary to obtain the same contribution to the error $\Delta I_{el}$ is inversely proportional to $P_0^2$ for various source-absorber combinations, other factors, such as the source activity, being equal. The contribution to $\Delta I_{el}$ by the number of counts with the absorber in resonance is more complex, since $I_R(2\theta)$ depends on both the value of $P_0$ and the scattering phenomenon. We will consider only two extreme cases. When the scattering is entirely inelastic, $t_R$ is proportional to the inverse square of $P_0$ as is $t_\infty$. If all the scattered intensity is elastic, $t_R$ is proportional to $(1 - P_0)/P_0^2$. Therefore, one should try to use source-absorber combinations with a value of $P_0$ as high as possible. For the source of $Co^{57}$ in the copper matrix, $P_0$ was equal to $0.6085 \pm 0.0018$ and decreased to about $0.5989 \pm 0.0023$ after about 8 months of use. The source with the chromium matrix had originally a value of $P_0 = 0.5740 \pm 0.0027$, but a constant increment of 0.27% every 10 days was observed. This slow increase, the origin of which is not known, was periodically checked and taken into account when elastic and inelastic intensities scattered by the crystal were evaluated.

The above figures of $P_0$ are average values over the active area of the source and the region of the absorber bathed by the direct beam. Since it was found with a previous $Co^{57}$ source in a copper matrix that $P_0$ did vary for different regions of the source, it could be argued that local variations of $P_0$ due to inhomogeneities of the source and of the absorber might affect the value of $I_{el}$ and, consequently, that of $I_{in}$. It can be shown that this objection is not valid provided that the elastic scattering power does not vary inside the region of the crystal bathed by the incident beam. Such a requirement was to a good approximation verified in all cases taken into consideration.

Three intensity measurements were done for each angular position of the crystal. One measurement was done without absorber, a second one with the absorber inserted in the scattered beam (and driven at resonant velocity in the case of the source in the copper matrix), and a third with an Al filter sufficiently thick to absorb all the 14.4-keV radiation. The last measurement, corrected for the attenuation of the hard radiation by the filter, was used to subtract the background from the other two intensities. The measurement with the absorber in the beam was also corrected for the photoelectric absorption by the absorber. This correction was determined by measuring the intensity of the direct beam transmitted through the absorber driven at infinite velocity, and was smaller than 15% of the intensity of the beam, with the absorbers used in the present work. All three measurements mentioned above were normalized by correcting them for the radioactive decay of the source. Finally, the cosmic and electronic background was periodically checked and deducted from each measurement.

Four different silicon crystals were used. Two of them (I and II) were lamellas cut from $P$-type (boron-doped) crystals of electrical resistivity equal to 20 and $6.5 \times 10^3\ \Omega$ cm, respectively, and with dislocation densities between $10^3$ and $10^4$ lines per $cm^2$; the growth axis of the crystals was $\langle 110 \rangle$ and the surfaces of the lamellas were cut perpendicularly to this axis. The lamella which was used for the measurements in the Laue-transmission

geometry was about 0.052 cm thick and was cut from the same crystal as lamella No. II. Another lamella III had surfaces of the {111} type and was cut from an $N$-type (phosphorous-doped) crystal, grown with the axis parallel to a ⟨111⟩ direction, of electrical resistivity equal to 12 Ω cm, and with less than $10^3$ dislocation lines per $cm^2$. The fourth crystal, which was used for the determination of the nuclear resonance absorption peak on the scattered beam and for the double Bragg scattering (see Sec. III), was grown with the axis parallel to a ⟨111⟩ direction, but its type and dislocation content were not known. All the silicon samples were chemically polished in CP-4 reagent. The aluminum crystals were lamellas with faces parallel to the {100}, {110}, and {111} planes, respectively. These lamellas were chemically polished after cutting by spark machining from bigger crystals of a purity better than 99.99%.

The crystal lamellas were large enough to intercept all the incident beam at the scattering angles used in the experiment. In many cases the scattered intensities were measured as a function of the angle between the incident beam and the crystal, which was rotated around the goniometer axis (see Figs. 2 and 3); the source and the counter were set at the scattering angle $2\theta_H$, equal to twice the Bragg angle for the reflection of interest, $H \equiv h, k, l$. Whenever the inelastic intensity only was needed, the measurements were done at the maximum of the Bragg peak, rather than for many settings of the crystal angle.

For silicon, intensities were also measured in the temperature range 80–600 °K, for the two reflections {444} and {555}. For this reason the crystal lamella was in a vacuum mounted on a metal frame, which was attached to a copper finger. This finger was either cooled by a coiled tubing where liquid nitrogen (or cold nitrogen vapors) was circulated, or heated by a small electric furnace. The temperature was held constant within ± 3 °K during each measurement.

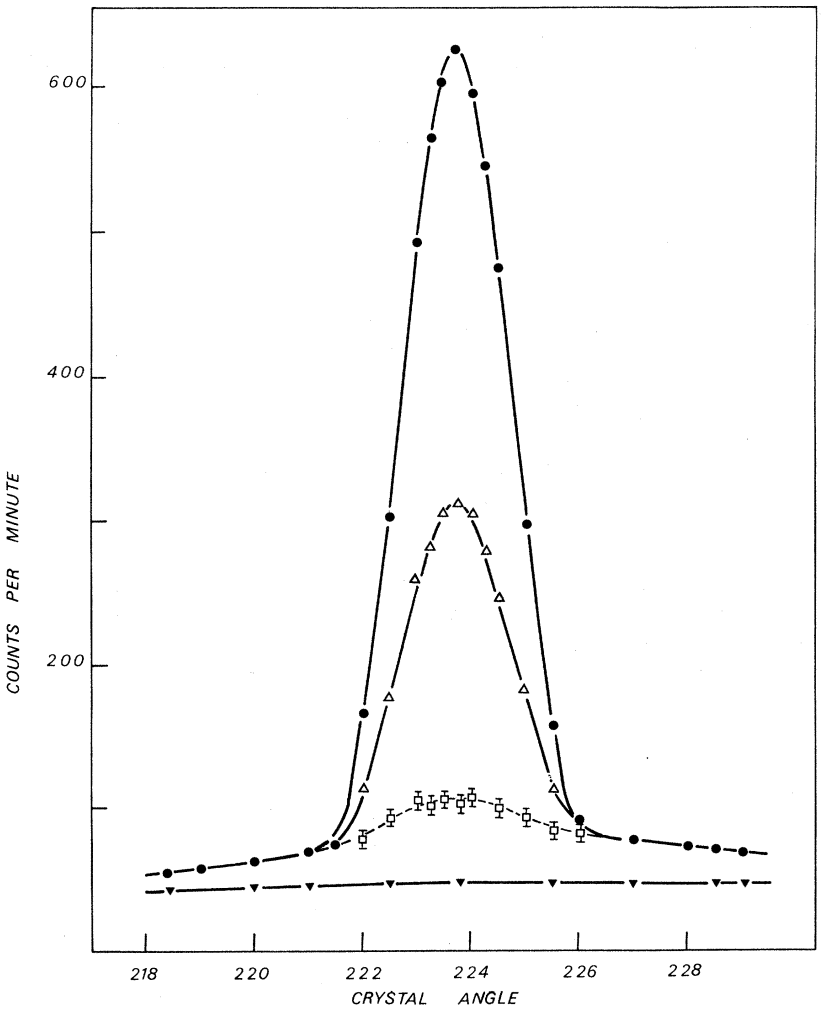


FIG. 2. Scattered intensities vs the glancing angle between incident beam and the surface of a silicon crystal, {220} reflection, Bragg geometry. Filled circles and open triangles are experimental points and correspond to the curves of $I_\infty$ and $I_R$ (Mössbauer absorber out of and in resonance, respectively). Open squares with the error bars were obtained from the two above sets of experimental data and correspond to the curve (dashed) of the inelastic intensity. The straight line under the curves is the hard gamma and cosmic background.

Integrated intensities of the elastic diffraction peaks were obtained by subtracting the area under the inelastic curve from that under the total intensity $I_\infty$, in plots such as those shown in Figs. 2 and 3. In many cases, however, the integration was done directly during the experiment. The crystal was rotated at a speed of about 1°/h through the whole angular range of the Bragg reflection by using a synchronous motor, and the total number of 14.4-keV photons scattered by the crystal was counted in the two cases, that is, with the absorber in and out of resonance with respect to the source. Absolute values of the elastic integrated intensities were obtained by measuring the intensity of the incident beam attenuated by calibrated Al filters.

The linear absorption coefficient $\mu$ of the 14.4-keV ($\lambda = 0.8602$ Å) radiation in silicon was found to be $\mu = 25.8 \pm 0.8$ cm$^{-1}$ by measuring the attenuation of the incident beam in three single-crystal lamellas. This value is in good agreement with that ($\mu = 25$ cm$^{-1}$) derived from the calculated cross sections for the photoelectric effect.[9]

### III. EXPERIMENTAL RESULTS AND DISCUSSION

Figures 2 and 3 illustrate the results obtained for the {220} and {444} reflections by silicon, respectively. The dashed curves, which have a peak at the Bragg angle, were derived from the top curve of $I_\infty$ and the middle curve of $I_R$ by applying formula (1) for the $I_{in}$. The base line corresponds to the background of hard gamma and cosmic radiations. In Fig. 3 the straight dashed line corresponds to the intensity of Compton scattering, which was calculated by using an expression previously reported[7] and the values of the incoherent scattering function given by Freeman.[10] Figure 2 illustrates the degree of precision in the inelastic intensity curve for a low-index reflection of a nearly perfect silicon

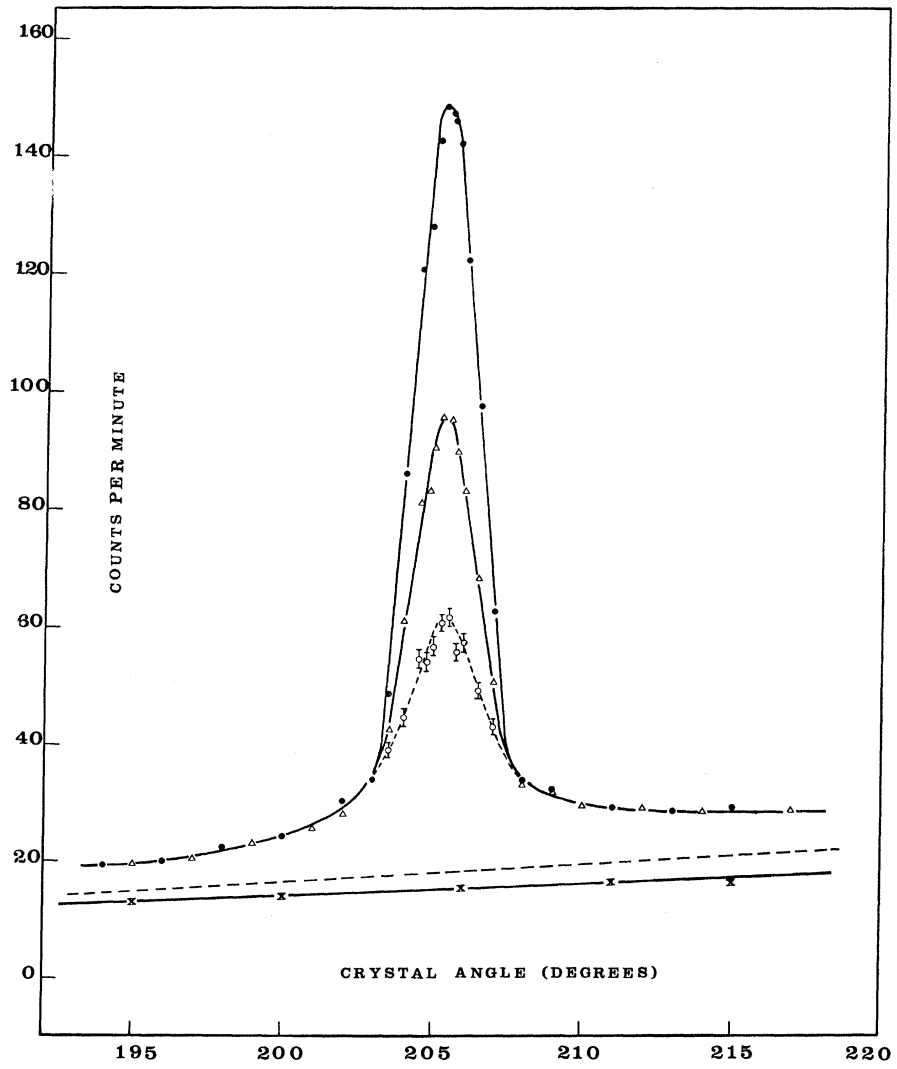


FIG. 3. Explanation is as for Fig. 2, except that the curves refer to the {444} reflection. The straight broken line is the intensity of the Compton scattering calculated as explained in the text.

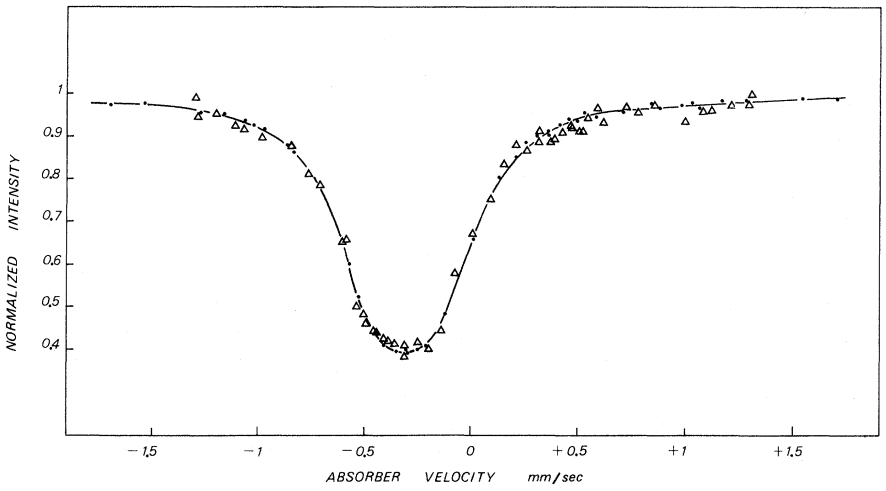


FIG. 4. Nuclear resonance absorption line with a $Co^{57}$ source in a copper matrix and a stainless-steel absorber enriched in $Fe^{57}$. Filled circles and open triangles are experimental points corresponding to absorption measurements on the incident beam and on the beam scattered by the {555} planes of a Si crystal, respectively. The two sets of points were normalized as explained in the text.

crystal. As shown by formulas (1) and (2), the relative precision of the inelastic intensity value is poor when most of the intensity is elastic. Although one can accumulate a great number of counts in order to determine $I_\infty$ and $I_R$ with great precision, confidence in the value of $I_{in}$ remains small, unless all the possible systematic errors are eliminated. The same conclusion applies to the value of the elastic intensity $I_{el}$ when most of the scattered intensity is inelastic.

The expression of the elastic and inelastic intensities given by the formulas (1) is based on the assumptions that (a) the nuclear resonance absorption peaks of the incident and scattered beams coincide on the energy scale, and (b) the resonance absorption lines of the incident and scattered beams have the same shape and width. These two points were checked by determining the resonance absorption line for the scattered beam at the peak of the {555} reflection by a silicon crystal. The results are reported in Fig. 4, together with points corresponding to an absorption experiment on the direct beam. The data on the scattered beam were normalized as follows: The value of $I_\infty(2\theta) - I_v(2\theta)/I_\infty(2\theta)$, where $I_v(2\theta)$ is the intensity transmitted at the relative velocity $v$ of the absorber, was multiplied by $P_0/P_{2\theta}$ in order to have two sets of points directly comparable. All the points superimpose on a single absorption curve. This fact proves that there is no energy shift or broadening for the recoilless radiation scattered by the crystal.

In the following all the elastic intensity corresponds to the diffracted (Bragg) intensity because elastic intensity was found only at the angle of the crystal reflections (see Figs. 2 and 3). A direct proof that the Bragg intensity is elastic was obtained by a double Bragg-scattering experiment, the geometry of which is illustrated in Fig. 5. A groove was cut into a single crystal of silicon in such a way that the surfaces of the groove were parallel to {111} planes. The intensity of the beam, after a double {444} reflection on the walls of the groove, was measured with and without the stainless-steel absorber inserted in the beam. This intensity was considerably lower than the elastic intensity after a single reflection because the crystal was not perfect. The double scattering acts as a filter for the intensity due to phonon scattering, and the twice-reflected beam is made only of contributions by Bragg diffraction. In fact, the intensity of the beam which is diffracted the first time by the crystal is of the same order of magnitude as the intensity of the incident beam, within the few seconds of arc corresponding to the Bragg reflection, whereas the intensity of the beam scattered by the phonons is, instead, six or seven orders of magnitude smaller than the incident beam. After the second scattering, the intensity of the phonon scattering is negligible with respect to that of Bragg diffraction. The result of this experiment was in agreement with the expectation because it was found that $P_{2\theta} = 0.6125 \pm 0.0211$ for the doubly scattered beam, which is in very good agreement with the value of $P_0 = 0.6085 \pm 0.0018$. This proves that all the diffracted intensity was elastic.

### A. Integrated Intensities of Diffraction Peaks

Experimental data on the integrated elastic intensities in the Bragg case were obtained as explained in Sec. II. In order to correct for slight asymmetries of the reflecting planes with respect to the surface of the crystal, all the measurements were repeated twice for two positions of the crystal in the beam. In the second position the crystal was rotated 180° around an axis perpendicular to the surface. The reported values of the elastic intensities are the averages of the data derived from the two sets of measurements. The results are

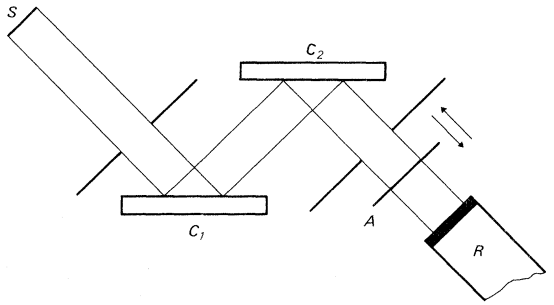


FIG. 5. Geometry of the double scattering experiment on a Si crystal. The experiment was done with the crystal set at the peak of the {444} reflection. *S*, *A*, and *R* are the Mössbauer source, absorber and detector, respectively. $C_1$ and $C_2$ are parts of the same crystal.

given in Table I for the silicon crystals and in Table II for the aluminum crystals. The errors are calculated by applying the law of error propagation to the statistical error pertaining to each measure. The calculated intensities of the perfect and mosaic crystals are also reported in the tables for the sake of comparison. The formula for the perfect crystal was that given by Hirsch and Ramachandran.[11] The values of the atomic scattering factors and of the dispersion corrections used for the calculations were those by Cromer and Waber[12] and by Cromer.[13] The Debye temperatures were $\Theta = 543\,^{\circ}\mathrm{K}$ for Si[14] and $\Theta = 395\,^{\circ}\mathrm{K}$ for Al.[15] In the case of the silicon samples the experimental intensities are somewhat higher, but much closer to the values of the perfect crystal than to those of the mosaic crystal. Sample No. IIa was an exception because measurements were intentionally done with the surface as cut by the diamond saw, with no chemical polishing. In the case of Al, instead, the experimental intensities are very close to those of the mosaic crystal.

TABLE I. Experimental and calculated values of the Bragg intensities for various reflections of silicon crystals. Symbols of the samples refer to the roman numerals given in Sec. II.

| | | Bragg intensity ($10^5$) | | |
|---|---|---|---|---|
| | | | Calculated | |
| *h k l* | Crystal symbol | Experimental | Perfect | Mosaic |
| 200 | Si I | 2.32 ± 0.25 | | |
| | Si II | 2.09 ± 0.20 | 1.624 | 39.77 |
| | Si IIa | 16.4 ± 0.09 | | |
| 333 | Si III | 0.494 ± 0.017 | 0.3901 | 4.383 |
| 440 | Si I | 0.798 ± 0.019 | 0.4642 | 6.621 |
| | Si II | 0.599 ± 0.018 | | |
| 444 | Si III | 0.300 ± 0.016 | 0.2723 | 3.041 |
| 660 | Si I | 0.247 ± 0.147 | 0.1372 | 1.262 |
| 555 | Si III | 0.120 ± 0.013 | 0.08685 | 0.5809 |

TABLE II. Experimental and calculated values of the Bragg intensities for various reflections of aluminum crystals.

| | Bragg intensity ($10^5$) | | |
|---|---|---|---|
| | | Calculated | |
| *h k l* | Experimental | Perfect | Mosaic |
| 222 | 13.7 ± 0.20 | 0.728 | 13.41 |
| 400 | 7.19 ± 0.15 | 0.5145 | 7.853 |
| 333 | 2.46 ± 0.05 | 0.2332 | 2.349 |
| 600 | 0.934 ± 0.027 | 0.1328 | 1.079 |
| 444 | 0.596 ± 0.032 | 0.08078 | 0.5077 |

### B. Intensity of Phonon Scattering at Bragg Angle

In the present work the relative values of the inelastic intensities at the maximum of the Bragg peaks are considered. Their behavior with the order of reflection and with temperature (in the case of silicon) is compared with that derived from the lattice wave theory of lattice vibrations. Absolute values of the phonon scattering will be discussed in a future paper. The experimental inelastic intensities were corrected for the effect of slight asymmetries of the crystallographic planes with respect to the surface of the crystal, as explained above. An example of the effect of the asymmetry is illustrated in Fig. 6, where the inelastic intensity corresponding to the {444} reflection is reported as a function of the aximuthal angle. The full line in the figure corresponds to the behavior calculated for an angle of 2° between the surface and the {111} planes. A back-reflection Laue photograph showed that this angle was, indeed, less than 3°.

The contribution of Compton scattering, which was calculated by using the Freeman incoherent functions for Si[10] and Al,[16] was subtracted from the total inelastic intensity unless otherwise specified. This correction amounted to a few percent at most in all the cases described in this paper.

Errors in the intensity of phonon scattering which are reported in the figures were calculated as explained above, in the case of the elastic intensities.

The formulas employed to calculate the intensity of phonon scattering are those of the lattice wave theory of thermal vibrations; they can be found in the books by James[17] and by Warren.[18] The most important formulas are briefly summarized below. The intensity of one-phonon scattering (first-order TDS) is the only one of interest for all the cases examined in the present work. On the assumption that the kinematical theory of diffraction applies to the phonon scattering, the first-order TDS for

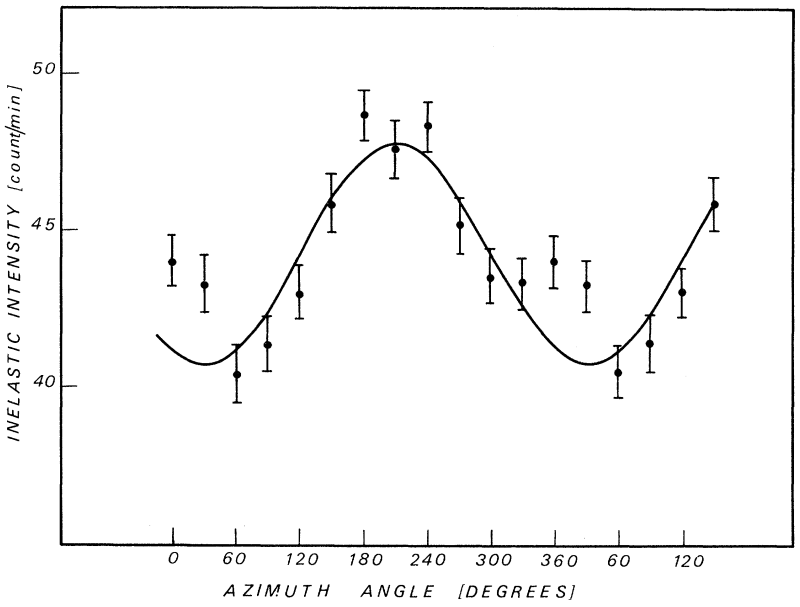


FIG. 6. Inelastic intensity vs the azimuthal angle (rotation around the surface normal) in the Bragg geometry, for the {444} reflection of Si. The solid line was calculated for an angle of 2° between lattice planes and surface of the crystal.

Bravais lattices is given in electron units per atom by the following formula:

$$(R_{\mathrm{TDS}})_{\tau_H} = |f_H^0|^2 e^{-2M_H}\, 2M_{\tau_H} \ , \tag{3}$$

where $f_H^0$ is the atomic scattering factor of the crystal with the atoms at rest, for the reflection $H \equiv h, k, l$; $e^{2M_H}$ is the square of the Debye-Waller factor, with $2M_H = \sum_{\omega_{\alpha j}} G_{\omega_{\alpha j}}$, the sum being extended to the entire Brillouin zone, that is to all the modes of the crystal; $\omega_{\alpha j}$ is the angular frequency of the mode; $\alpha$ is the index of the branch; and the index $j$ is for the three polarization directions (one longitudinal and two transverse). $2M_{\tau_H} = (\sum_{\omega_{\alpha j}} G_{\omega_{\alpha j}})_{\tau_H}$ is a partial sum extended to all the modes for which the end points of the wave vectors fall inside the volume $\tau_H$. This volume corresponds to the volume of the reciprocal lattice over which the TDS intensity is integrated; $\tau_H$ is determined by the geometry of the scattering experiment as explained below. The explicit expression of $2M_{\tau_H}$ is

$$2M_{\tau_H} = \frac{8\pi^2\hbar}{mN_c}\left(\frac{\sin\theta_H}{\lambda}\right)^2 \times \sum_{\alpha,j} \int_{\tau_H} \frac{w(\vec{q}_{\alpha j})\,(\langle n_{\omega_{\alpha j}}\rangle + \tfrac{1}{2})\cos^2(S, e_{q_{\alpha j}})\, d\tau}{\omega_{\alpha j}},$$

where $\hbar$, $m$, and $N_c$ are the reduced Planck's constant, the atomic mass, and the number of primitive unit cells per unit volume, respectively; $\lambda$ and $\theta_H$ are the wavelength of the radiation and the Bragg angle for the reflection $H \equiv h, k, l$; $\vec{q}_{\alpha j}$ is the wave vector of the phonon, $|\vec{q}_{\alpha j}| = \omega_{\alpha j}/v_{\vec{q}_{\alpha j}}$, $v_{\vec{q}_{\alpha j}}$ being the velocity of the wave; $w(\vec{q}_{\alpha j})$ is a weight function for the distribution of the intensity in the incident beam, which is not uniform in the various directions defined by the size of the source and the slit on the incident beam; $\cos(S, e_{q_{\alpha j}})$ is the cosine of the angle between the scattering vectors $\vec{S}$, $|\vec{S}| = 2\sin\theta_H$, and the unit vector $\vec{e}_{q_{\alpha j}}$ in the polarization direction of the phonon $\vec{q}_{\alpha j}$.

The contributions of the acoustical and optical phonons to $2M_{\tau_H} = 2M^{\mathrm{ac}}_{\tau_H} + 2M^{\mathrm{opt}}_{\tau_H}$ were evaluated separately[7] as follows:

$$2M^{\mathrm{ac}}_{\tau_H} = \frac{8\pi^2 kT}{mN_c}\left(\frac{\sin\theta_H}{\lambda}\right)^2 \sum_j \frac{1}{v_j^2} \times \int_{\tau_H} \frac{w(\vec{q}_j)\cos^2(S, e_{q_j})\, d\tau}{\vec{q}_j^{\,2}}, \tag{4}$$

$$2M^{\mathrm{opt}}_{\tau_H} = \frac{8\pi^2\hbar}{mN_c}\left(\frac{\sin\theta_H}{\lambda}\right)^2 \frac{(\langle n_{\omega_R}\rangle + \frac{1}{2})}{\omega_R} \times \sum_j \int_{\tau_H} w(\vec{q}_j)\cos^2(S, e_{q_j})\, d\tau \ . \tag{5}$$

Formula (4), which applies to both aluminum and silicon, was obtained with the following approximations: (a) Dispersion effects are absent in the acoustical branches. This fact was checked against the dispersion curves obtained by neutron inelastic scattering experiments.[19] (b) we have $\hbar\omega_j \ll kT$, then $\langle n_{\omega_j}\rangle + \frac{1}{2} \approx kT/\hbar\omega_j$. This fact is valid for all acoustical frequencies for which the end point of the wave vector falls inside the volume $\tau_H$; (c) The solid was assumed to be elastically isotropic, that is $v_{\vec{q}_j} = v_j$. For the main crystallographic directions the velocities of the longitudinal and of the transverse waves are fairly constant.

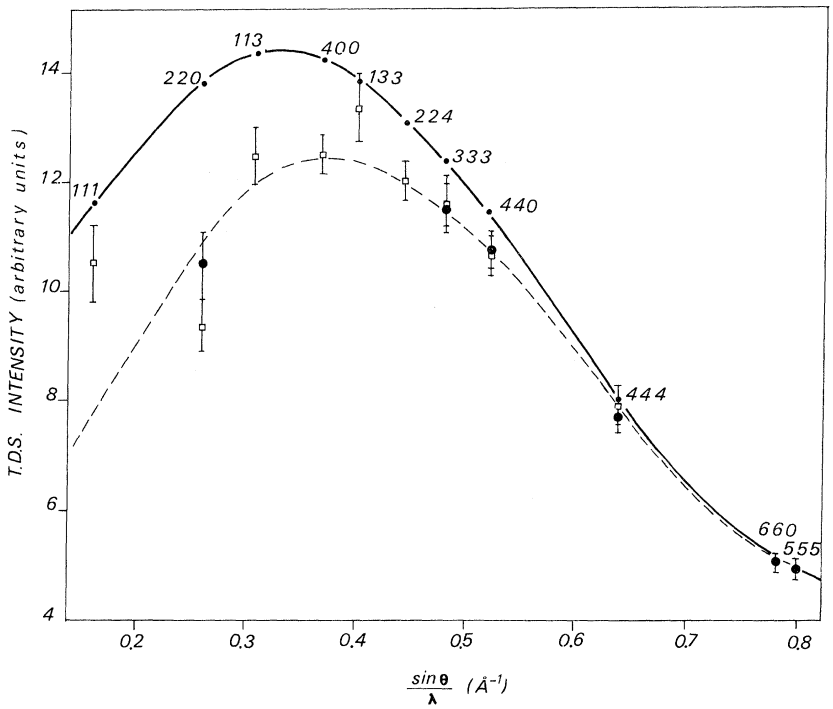


FIG. 7. Thermal diffuse scattering intensity vs $\sin\theta/\lambda$ for various reflections of different Si crystals. Filled circles and open squares, which were obtained with the reflection and transmission geometries, respectively, are experimental data with the statistical error bars. Solid and dashed curves were calculated by using the spherical and cylindrical approximations, respectively, for the shape of the volume $\tau_H$ where the TDS intensity was integrated. See the text for further information on the fitting of the calculated curves with the experimental points.

In addition, the two transverse waves have roughly the same velocity even when symmetry rules do not require it. However, variations of the TDS intensity with the azimuthal angle were experimentally investigated for silicon in the Bragg geometry. A change in the crystal azimuth corresponds to a rotation of the volume $\tau_H$ around the scattering vector $\vec{S}$ in reciprocal space. Figure 6 shows that the observed variations of the intensity can be explained by the asymmetry of the crystallographic planes. When no asymmetry was present, the inelastic intensity did not vary with the azimuth. Since the TDS intensity is not affected by the orientation of the $\tau_H$ volume in reciprocal space, the approximation made by taking a value of $v_{\vec{q}j}$ averaged over all the directions of the $\vec{q}$ vector is acceptable. The values of the velocities which were used for the evaluation of (4) were those of the polycrystalline solid.[20] That is, $v_l = 8.945\times10^5$ cm/sec and $v_t = 5.341\times10^5$ for the longitudinal and transverse modes, respectively, in the case of silicon; $v_l = 6.61\times10^5$ cm/sec and $v_t = 3.17\times10^5$ cm/sec in the case of aluminum. Formula (5), which applies to silicon only, was derived with the assumption that the optical waves have a constant angular frequency $\omega_R$, an approximation which is justified by the strong dispersion effects of the optical branch at $\vec{q}=0$. The frequency $\nu_R = 15.3\times10^{12}$ Hz, which was used for the numerical calculation of (5), was taken from the neutron scattering data.[19]

As mentioned above, the size and shape of the reciprocal lattice volume $\tau_H$ is determined by the scattering geometry. It can be written to a good approximation, as

$$\tau_H \approx \frac{\Delta\alpha_1\,\Delta\alpha_2\,\Delta\alpha_3}{\lambda^3}\sin2\theta_H\ , \qquad (6)$$

where $\Delta\alpha_1$ is the horizontal divergence of the incident beam and $\Delta\alpha_2$, $\Delta\alpha_3$ are the horizontal and vertical divergences, respectively, of the scattered beam accepted by the counter. For silicon two approximations on the shape of volume $\tau_H$ were made in order to calculate the integrals in formulas (4) and (5). In one case the volume $\tau_H$ was replaced by a sphere with a radius $R=(3\tau_H/4\pi)^{1/3}$ centered on the reciprocal lattice node $H$. In the other case $\tau_H$ was replaced by a straight cylinder with the height equal to $\Delta\alpha_1\sin2\theta_H/\lambda$ and radius equal to $(\Delta\alpha_2\Delta\alpha_3/\pi)^{1/2}(1/\lambda)$. Only the spherical approximation was used for aluminum. In all cases the weight function $w(\vec{q}_j)$ was approximated with the linear function $1\text{-}q\cos\eta/q_{\max}$, where $\eta$ is the polar angle (see the Appendix). From a check of shape of the incident beams and of the diffraction peaks it was found that this approximation was satisfactory. Details on the calculations of integrals in formulas (4) and (5) can be found in the Appendix. For all the Si reflections the value of $2M^{\rm opt}$ was less than 5% of $2M^{\rm ac}$.

Figure 7 illustrates the dependence of the TDS relative intensities of silicon vs $\sin\theta/\lambda$ for a number of lattice reflections, in both the Bragg and Laue geometries. The data in the Laue geometry were first divided by $2\mu/te^{-\mu t}$, where $t=t_0/\cos\theta_H$,

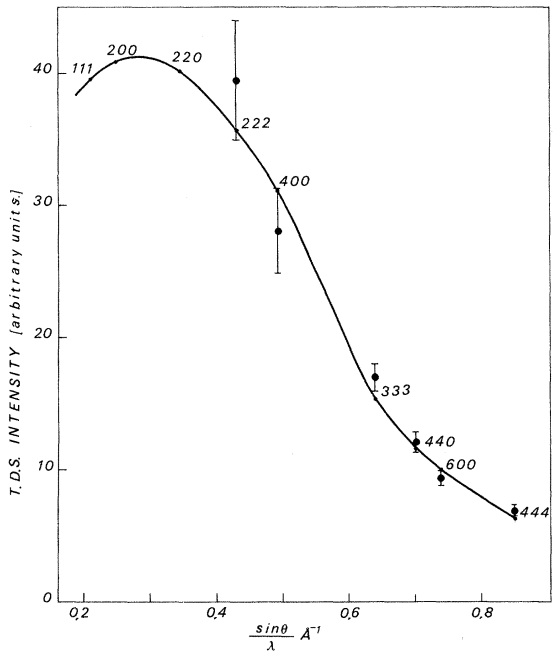


FIG. 8. Thermal diffuse scattering intensity vs $\sin\theta/\lambda$ for various reflections of three Al crystals. The filled circles are experimental points with the statistical error bars. The solid line was calculated by assuming that the volume where the TDS intensity was integrated was a sphere.

$t_0$ being the thickness of the crystal, and then they were multiplied by a factor which was the average of the ratios between the TDS intensities in the Bragg and Laue cases, for the {333}, {440}, and {444} reflections. In addition, the intensities of the odd reflections were multiplied by 2 in order to have figures comparable to the calculated ones. The solid and dashed lines were calculated by using formula (3) with the values of $2M_{\tau_H}$ obtained from (4) and (5). The expression in (3) was multiplied by $(1+\cos^2 2\theta_H)/\sin 2\theta_H$ to take into account the angular dependence of the intensity due to the polarization of the scattered beam and to the size of the volume element in reciprocal space. The upper and lower curves in Fig. 7 were calculated by using the spherical and cylindrical approximations, respectively, for the volume $\tau_H$. The two calculated curves were fitted to the experimental data by forcing the curves to go through the experimental point of the {555} reflection. Although there is some scatter among the experimental points of the low-index reflections (for which the inelastic intensity is a small fraction of the total intensity), the experimental behavior is in better agreement with the curve calculated by using the cylindrical approximation. Figure 8 illustrates the dependence of the TDS intensities on $\sin\theta_H/\lambda$ for aluminum in the Bragg geometry. The solid curve, which was obtained by using the spherical approximation for $\tau_H$, was fitted on the experimental points corresponding to the high-order reflections. The agreement is quite satisfactory, probably because the data at small values of $\sin\theta_H/\lambda$ are not available and the errors on the intensities of the {222} and {400} reflections are large.

The dependence of the TDS intensity on temperature was tested for the two reflections {444} and {555} of the Si crystal No. III, in the temperature range 80–600 °K. The symmetric Bragg geometry was used in both cases. The relative values of the

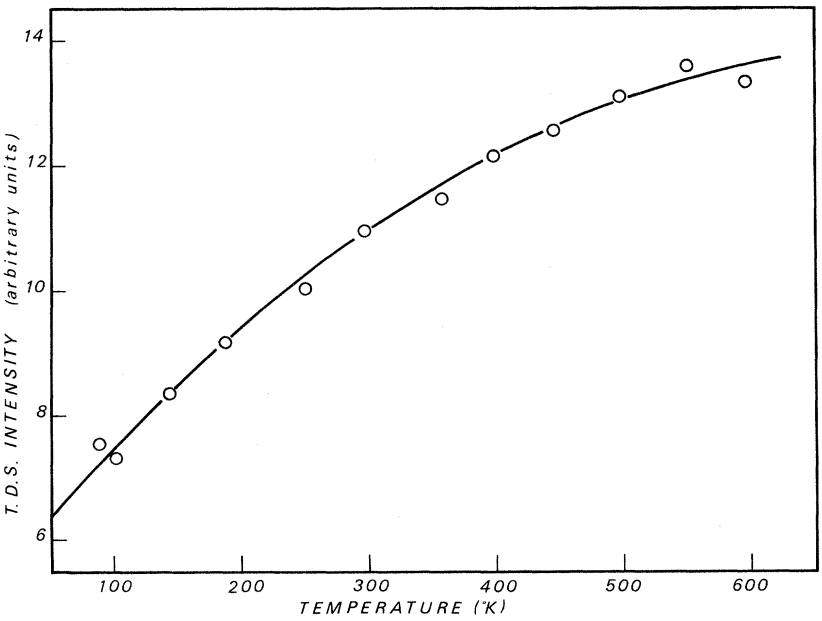


FIG. 9. Thermal diffuse scattering intensity vs absolute temperature for the {444} reflection of a Si crystal. Open circles are the experimental points. The solid line is the temperature dependence of the TDS intensity calculated as explained in the text.

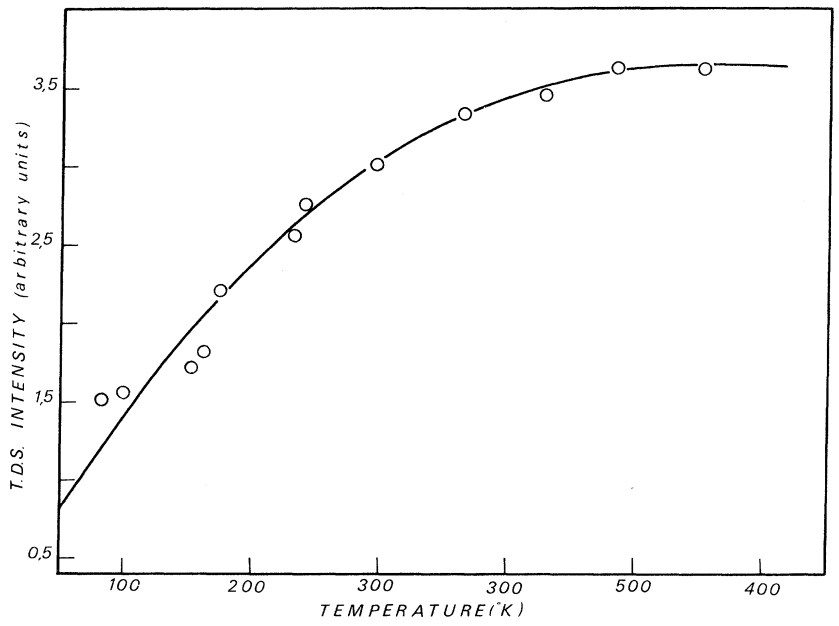


FIG. 10. Explanation is as for Fig. 9, except that the open circles and the solid curve refer to the {555} reflection.

experimental intensities are reported in Figs. 9 and 10, together with the data calculated by using the temperature dependence (approximately proportional to $Te^{-2M}$) of the intensity scattered by the modes of the crystal. The agreement between experimental and calculated data is very good for both reflections.

## IV. SUMMARY

The intensities of the 14.4-keV ($\lambda = 0.8602$ Å) $\gamma$ rays, from two $Co^{57}$ sources, scattered by various Si and Al crystals, were measured for different orientations of the crystals and of the detector with respect to the incident beam. The elastic and inelastic parts of the scattered intensities were separated one from the other by using nuclear resonance absorption. The most significant results are the following: (a) A comparison between the nuclear resonance absorption curves of the scattered beam at the peak of the Si {555} reflection and of the direct beam shows that there is no energy shift or broadening of the absorption peak for the scattered beam. A double Bragg-scattering experiment with Si crystal indicates that all the diffracted intensity is elastic. (b) The angle dependence of the experimental intensities of TDS at the Bragg peaks was investigated for various reflections of Si and Al crystals, and a comparison was done on a relative scale with the data calculated by using the lattice wave theory of TDS intensities. For the calculations it is assumed that the solid is elastically isotropic and that the reciprocal lattice volume $\tau_H$, over which the diffuse scattering is integrated, has either a spherical or cylindrical shape. The experimental behavior for Si is in agreement with the curve calculated by using the cylindrical approximation for $\tau_H$, while for Al the spherical approximation of $\tau_H$ is sufficient. (c) The temperature dependence of the TDS intensities corresponding to the peaks of the {444} and {555} reflections of a Si crystal was investigated in the temperature range 80–600 °K. The agreement with the calculated dependence of the TDS intensity is very good on a relative scale.

## APPENDIX

The reciprocal lattice volume $\tau_H$, where the expression of the TDS intensity is integrated, is a parallelepiped with slightly curved faces. Figure 11 illustrates a section of this volume with the scattering plane.

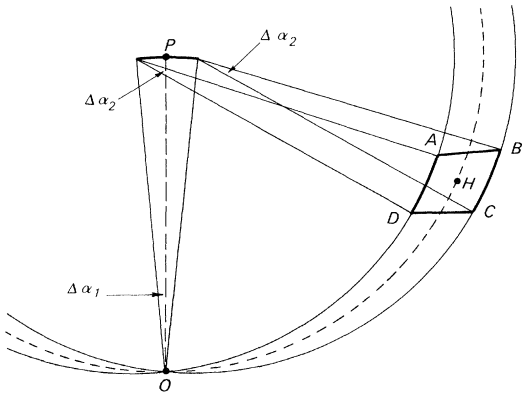


FIG. 11. Scattering geometry in the reciprocal space. The figure is the section with the scattering plane. $O$ and $H$ are the origin and the node $H \equiv h, k, l$ of the reciprocal lattice, respectively. $ABCD$ is the section of the volume $\tau_H$ where the TDS intensity was integrated.

In the spherical approximation the volume $\tau_H$ is replaced with a sphere of equal volume, centered on the reciprocal lattice node $H$. Spherical polar coordinates are used, with the polar axis perpendicular to the scattering vector $\vec{S}$ in the scattering plane.

It follows that

$$w(\vec{q}) = 1 - q\cos\eta/q_m \ ,$$

where $q_m/2\pi$ is the radius of the sphere, and

$$\cos(S, e_q) = \begin{cases} \sin\eta\cos\varphi & \text{for longitudinal vibrations} \\ -\cos\eta \quad \cos\varphi \\ -\sin\varphi \end{cases} \text{for transverse vibrations} \ .$$

The integrals in formulas (4) and (5) can now be written as

$$\frac{1}{8\pi^3}\int_{\tau_H}\left(1-\frac{q\cos\eta}{q_m}\right)\cos^2(S,e_q)\sin\eta\, dq\, d\eta\, d\varphi \ ,$$

$$\frac{1}{8\pi^3}\int_{\tau_H}\left(1-\frac{q\cos\eta}{q_m}\right)\cos^2(S,e_q)\, q^2\sin\eta\, dq\, d\eta\, d\varphi \ .$$

After substitution of the proper expression for $\cos(S, e_q)$ the above integrals are solved analytically with the following results:

$$\sum_j \frac{1}{v_j^2}\int_{\tau_H}\frac{w(\vec{q}_j)\cos^2(S,e_{qj})\,d\tau}{\vec{q}_j^{\,2}} = \frac{q_m}{96\pi^2}\left(\frac{13}{v_l^2}+\frac{23}{v_t^2}\right) ,$$

$$\sum_j \int_{\tau_H} w(\vec{q}_j)\cos^2(S,e_{q_j})\,d\tau = \frac{5q_m^3}{48\pi^2} = \frac{5\tau_H}{8} \ ,$$

where $v_l$ and $v_t$ are the velocities of longitudinal and transverse vibrations, respectively.

In the cylindrical approximation, the volume $\tau_H$ is replaced with a straight cylinder, the base of which has an area equal to $\pi\rho_m^2$, where $\rho_m = (1/\lambda) \times (\Delta\alpha_2\Delta\alpha_3/\pi)^{1/2}$ and the height $2z_m$ is equal to $(\Delta\alpha_1 \sin 2\theta_H)/\lambda$ (see formula 6 for the symbols). We have then

$$w(\vec{q}) = 1 - z/z_m \ ,$$

$$\cos(S, e_q) = \begin{cases} \dfrac{\rho}{(\rho^2+z^2)^{1/2}\cos\varphi} & \text{for longitudinal vibrations} \\ \dfrac{-z}{(\rho^2+z^2)^{1/2}\cos\varphi} \\ -\sin\varphi \end{cases} \text{for transverse vibrations} \ .$$

The integral in (4) is written

$$\frac{1}{4\pi^2}\int_{\tau_H}\left(1-\frac{z}{z_m}\right)\cos^2(S,e_q)\,\frac{\rho}{\rho^2+z^2}\,d\rho\, dz\, d\varphi \ ,$$

and similarly for the integral of (5). The analytical solution of these integrals is as follows:

$$\sum_j \frac{1}{v_j^2}\int_{\tau_H}\frac{w(\vec{q}_j)\cos^2(S,e_{qj})\,d\tau}{\vec{q}_j^{\,2}} = \frac{1}{4\pi}\left[\rho_m \arctan\frac{q_m}{\rho_m}\left(\frac{1}{v_l^2}+\frac{3}{v_t^2}\right) + \frac{z_m}{2}\ln\left(1+\frac{\rho_m^2}{z_m^2}\right)\left(\frac{1}{v_l^2}+\frac{1}{v_t^2}\right) - \frac{\rho_m^2}{z_m}\ln\left(1+\frac{z_m^2}{\rho_m^2}\right)\frac{1}{v_t^2}\right] ,$$

$$\sum_j \int_{\tau_H} w(\vec{q}_j)\cos^2(S,e_{q_j})\,d\tau = \pi\rho_m^2 z_m = \tfrac{1}{2}\tau_H \ .$$


[1] W. Cochran, Acta Cryst. A25, 95 (1969).

[2] C. B. Walker and D. R. Chipman, Acta Cryst. A26, 447 (1970).

[3] L. D. Jennings, Acta Cryst. A26, 613 (1970).

[4] K. D. Rouse and M. J. Cooper, Acta Cryst. A25, 615 (1969).

[5] G. Caglioti, Nuovo Cimento Suppl. 5, 1177 (1967).

[6] D. A. O'Connor and N. M. Butt, Phys. Letters 7, 233 (1963).

[7] C. Ghezzi, A. Merlini, and S. Pace, Nuovo Cimento 64B, 103 (1969).

[8] F. Parak, R. L. Mössbauer, and W. Hoppe, Ber. Bunsenges. 74, 1207 (1970).

[9] H. A. Bethe and E. E. Salpeter, in *Encyclopedia of Physics*, edited by S. Flügge (Springer, Berlin, 1957), Vol. 35, p. 390.

[10] A. J. Freeman, Acta Cryst. 12, 929 (1959).

[11] P. B. Hirsch and G. N. Ramachandran, Acta Cryst. 3, 187 (1950).

[12] D. T. Cromer and J. T. Waber, Acta Cryst. 18, 104 (1965).

[13] D. T. Cromer, Acta Cryst. 18, 17 (1965).

[14] B. W. Batterman and D. R. Chipman, Phys. Rev. 126, 1461 (1962).

[15] R. M. Nicklow and R. A. Young, Phys. Rev. 152, 591 (1966).

[16] A. J. Freeman, Phys. Rev. 113, 176 (1959).

[17] R. W. James, *The Optical Principles of the Diffraction of X-rays* (G. Bell and Sons, London, 1957), see Chap. V.

[18] B. E. Warren, *X-Ray Diffraction* (Addison-Wesley, New York, 1969), see Chap. XI.

[19] B. N. Brockhouse, Phys. Rev. Letters 6, 256 (1959).

[20] O. L. Anderson, in *Physical Acoustic*, edited by W. P. Mason (Academic, New York, 1965), Vol. 3, Part B, p. 84.